

A Dynamic Water Channel Affects O₂ Stability in [FeFe]-Hydrogenases

Claudia Brocks,^[a] Chandan K. Das,^[b] Jifu Duan,^[a] Shanika Yadav,^[c] Ulf-Peter Apfel,^[c] Subhasri Ghosh,^[a] Eckhard Hofmann,^[d] Martin Winkler,^[e] Vera Engelbrecht,^[a] Lars V. Schäfer,^{*[b]} and Thomas Happe^{*[a]}

[FeFe]-hydrogenases are capable of reducing protons at a high rate. However, molecular oxygen (O₂) induces the degradation of their catalytic cofactor, the H-cluster, which consists of a cubane [4Fe₄S] subcluster (4Fe_H) and a unique diiron moiety (2Fe_H). Previous attempts to prevent O₂-induced damage have focused on enhancing the protein's sieving effect for O₂ by blocking the hydrophobic gas channels that connect the protein surface and the 2Fe_H. In this study, we aimed to block an O₂ diffusion pathway and shield 4Fe_H instead. Molecular dynamics (MD) simulations identified a novel water channel (W_H) surrounding the H-cluster. As this hydrophilic path may be

accessible for O₂ molecules we applied site-directed mutagenesis targeting amino acids along W_H in proximity to 4Fe_H to block O₂ diffusion. Protein film electrochemistry experiments demonstrate increased O₂ stabilities for variants G302S and S357T, and MD simulations based on high-resolution crystal structures confirmed an enhanced local sieving effect for O₂ in the environment of the 4Fe_H in both cases. The results strongly suggest that, in wild type proteins, O₂ diffuses from the 4Fe_H to the 2Fe_H. These results reveal new strategies for improving the O₂ stability of [FeFe]-hydrogenases by focusing on the O₂ diffusion network near the active site.

Introduction

[FeFe]-hydrogenases efficiently catalyze the reversible reduction of protons to molecular hydrogen (H₂) at low overpotentials with remarkably high turnover frequencies.^[1] However, technological applications for enzymatic fuel production are severely hampered by the extreme O₂ sensitivity of the unique [6Fe-6S]

cofactor (H-cluster) of [FeFe]-hydrogenases.^[2] It consists of two subclusters, a unique binuclear diiron-moiety (2Fe_H) and a [4Fe₄S] cubane (4Fe_H) which are covalently linked by a bridging cysteine (Cys) residue^[3] (Figure 1). The two iron atoms of 2Fe_H, referred to as distal (Fe_d) and proximal (Fe_p) depending on their distance to the 4Fe_H subsite, are coordinated by two CN⁻ (cyanide) and three CO (carbon monoxide) ligands, and one of the latter bridges Fe_p and Fe_d. In addition, Fe_p and Fe_d are bridged by an azadithiolate (adt) ligand (Figure S3A). Its nitrogen bridgehead is in H-bonding distance to an amino acid, which could transfer protons. It is part of a proton transfer pathway connecting the protein surface and the active site.^[4-6]

The mechanisms of how O₂ destroys the H-cluster have been extensively studied in recent years. O₂ enters the gas channel network of the enzyme, diffuses into the deeply buried active site pocket and binds to the substrate coordination site at Fe_d where it initiates reactions that result in the irreversible degradation of the H-cluster.^[7] The activation of O₂ at Fe_d leads to the formation of reactive oxygen species (ROS).^[8,9] First superoxide (O₂⁻) is formed, which can be protonated through the native proton transfer pathway, yielding a hydroperoxo intermediate (Fe_d-HO₂).^[10,11] From here, two different degradation processes can be initiated. Another protonation event may lead to a disproportionation that causes the release of a water molecule and yields an iron-oxo species (Fe_d(IV)=O²⁻). The latter reacts with the nearby CO and CN⁻ ligands that are released as CO₂ or OCN⁻, respectively. The lost Fe_d ligands are replaced by water molecules in a stepwise manner, finally leading to the complete solvation of Fe_d. By following the anomalous electron density in crystals of the [FeFe]-hydrogenase Cpl from *Clostridium pasteurianum* that were exposed to moistened air^[14] it could be confirmed that the 2Fe_H subcluster first loses Fe_d while Fe_p remains attached to the 4Fe_H

[a] Dr. C. Brocks, Dr. J. Duan, S. Ghosh, Dr. V. Engelbrecht, Prof. Dr. T. Happe
Faculty of Biology and Biotechnology, Photobiotechnology
Ruhr University Bochum
Universitätsstrasse 150, 44801 Bochum (Germany)
E-mail: thomas.happe@rub.de

[b] Dr. C. K. Das, Prof. Dr. L. V. Schäfer
Faculty of Chemistry and Biochemistry, Center for Theoretical Chemistry
Ruhr University Bochum
Universitätsstrasse 150, 44801 Bochum (Germany)
E-mail: lars.schaefer@ruhr-uni-bochum.de

[c] S. Yadav, Prof. Dr. U.-P. Apfel
Faculty of Chemistry and Biochemistry, Inorganic Chemistry
Ruhr University Bochum
Universitätsstrasse 150, 44801 Bochum (Germany)

[d] Prof. Dr. E. Hofmann
Faculty of Biology and Biotechnology, X-ray structure analysis of proteins
Ruhr University Bochum
Universitätsstrasse 150, 44801 Bochum (Germany)

[e] Dr. M. Winkler
Electrobiotechnology
TUM Campus Straubing
Schulgasse 22, Straubing 94315 (Germany)

Supporting information for this article is available on the WWW under <https://doi.org/10.1002/cssc.202301365>

© 2023 The Authors. ChemSusChem published by Wiley-VCH GmbH. This is an open access article under the terms of the Creative Commons Attribution Non-Commercial NoDerivs License, which permits use and distribution in any medium, provided the original work is properly cited, the use is non-commercial and no modifications or adaptations are made.

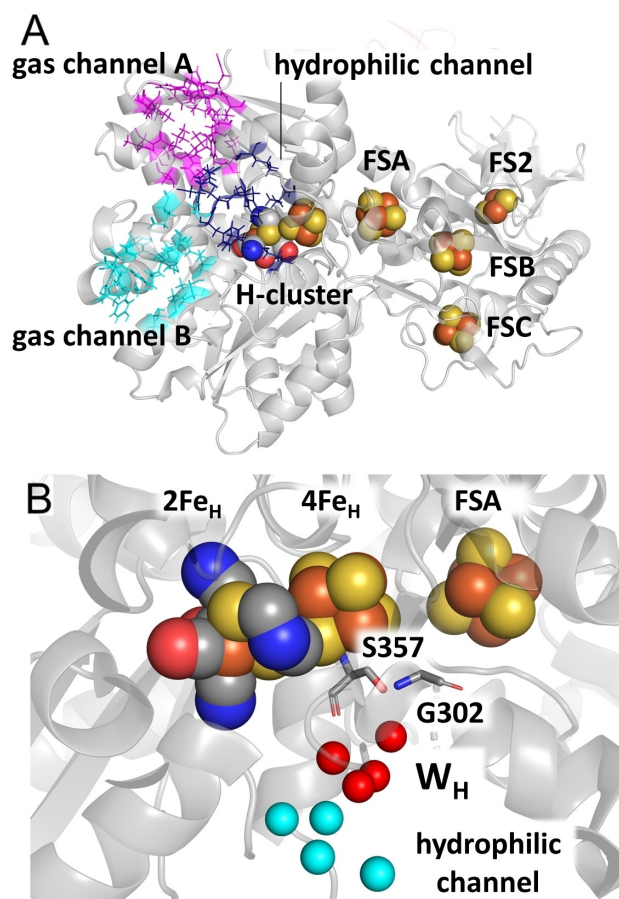


Figure 1. A. Cartoon structure of Cpl (4XDC)^[12] from *Clostridium pasteurianum*. The hydrophobic gas channels A (magenta) and B (cyan), the hydrophilic channel (blue), the H-cluster (4Fe_H and 2Fe_H) and all accessory FeS-clusters are highlighted. B. Location of structurally conserved crystal water molecules belonging to a hydrophilic channel (cyan spheres)^[13] and W_H (red spheres). Redox clusters are depicted as spheres (Fe: brown, S: yellow, N: blue, O: red, C: grey) (The H-cluster is shown in detail in Figure S3A).

moiety.^[8,14,15] In addition, a second long-suspected^[16,17] degradation event was confirmed which mainly affects the 4Fe_H subcluster.^[14,18]

If the protonation of the hydroperoxo ligand at the 2Fe_H subcluster leads to the release of, for example, a hydrogen peroxide (H₂O₂) molecule, this free ROS species can reach the 4Fe_H site by diffusion and attack the Cys ligands of two Fe-sites in the 4Fe_H cluster architecture (C503 and C355 in Cpl (Figure S3A)) causing its transformation into a [2Fe2S]-cluster. According to theoretical studies, the diffusing ROS species could be H₂O₂, a perhydroxyl (OOH•) or a hydroxyl (OH•) radical.^[8,9,16]

The degree of H-cluster degradation after exposure to O₂ depends on several mechanisms that are determined by individual structural features that explain why the level of O₂ sensitivity varies for different [FeFe]-hydrogenases. For example, the extent of O₂ sensitivity is influenced by the velocity of O₂ diffusion along and by the numbers of O₂ diffusion pathways to the active site, by the presence of accessory [FeS]-clusters, by the rates of proton delivery to the active site, by specific features of the protein environment near the active site, or by

co-solvents that enable sulfide-mediated inactive states.^[2,10,11,13,17,19,20] Based on the beneficial properties of various natural [FeFe]-hydrogenases identified so far, several attempts have been made to modify the sequences of [FeFe]-hydrogenases accordingly.

The three most common strategies to alleviate the O₂ sensitivity of hydrogenases are i) to enhance the molecular sieve effect within the gas channel system, ii) to accelerate the electron flow to the H-cluster to allow rapid reduction of O₂ to water, or iii) to modify the direct protein environment of the H-cluster in order to decrease the binding affinity for O₂.^[13,17,21,22,23] While the latter two strategies require a series of well-designed modifications of amino acids at the highly sensitive interface between the catalytic cofactor and its electron and proton delivery pathways, the modification of gas channels appears to be more straightforward. The gas channel network of hydrogenases consists of hydrophobic cavities interconnected by smaller passages that lead to a larger central cavity at the O₂ sensitive active site. Molecular dynamics (MD) simulations, crystal structure analyses and site-directed amino acid exchange experiments have shown that there are two main branches of gas channels, gas channel A and B (Figure 1A) in the protein domain that harbors the active site. Manipulations of these two channels with the aim of increasing the O₂ stability have so far achieved only limited success.^[7,24,25] Indeed, the idea of two continuous and static hydrophobic gas channels that lead to the central cavity of the 2Fe_H subsite, as deduced from rigid crystal structures, probably oversimplifies matters. It has been discussed that molecular motions within the protein can allow diatomic molecules such as O₂ or CO to 'hop' from one cavity to the next, instead of diffusing through permanently accessible channels.^[7] Overall, the possible presence of multiple interconnected gas channels in [FeFe]-hydrogenases or allosteric communication between O₂ binding sites makes strategies to prevent O₂ diffusion to the active site quite challenging.

Hydrophobic O₂ molecules can also diffuse along hydrophilic (water-filled) channels that exist within protein matrices,^[13,16,21,25] although this has not yet been shown for [FeFe]-hydrogenases. In Cpl, a hydrophilic channel (also known as 'wet channel') (Figure 1), defined by protein-coordinated water molecules and conserved amino acids, consists of two subchannels: one starts at the surface-exposed residue K571, the other at E361, which is in the vicinity of the H-cluster.^[5,13] This united hydrophilic channel leads to the central cavity.

In this work, we combined MD simulations and a classical site-directed mutagenesis approach to prevent the diffusion of water to the 4Fe_H subcluster, and thereby the destruction of the H-cluster by O₂, in the [FeFe]-hydrogenase Cpl from *C. pasteurianum*. We focused on dynamic channels in the direct vicinity of the H-cluster, targeting a newly identified channel connecting the 4Fe_H and the 2Fe_H subclusters. Local blocking of this channel by replacing residue G302 (Figure 1B) by serine was confirmed by MD simulations based on a high-resolution crystal structure of the G302S variant. Additionally, MD simulations, electrochemistry and crystallography provide mechanistic insights into the reported O₂ stability of Cpl variant

S357T by exploiting structural rigidity at position 357 and its proximity to the hydrophobic side-chain of L192.

Results and Discussion

Monitoring the water channel network in the vicinity of the active site

To identify hydrated channels in the protein matrix, a model of wild type (WT) Cpl was generated based on its X-ray crystal structure 4XDC.^[12] The protein was simulated for a total of 3000 ns of all-atom MD simulation in explicit water (see Supporting Information). The simulations revealed a network of tunnel-shaped cavities connecting the active site with the protein surface (Figure 1, Figure S3B). These cavities are consistent with the existence of a water channel ending close to the active site cavity, as observed in the X-ray crystal structure of Cpl, which shows water molecules assigned to the hydrophilic channel.^[13] The dynamic water channels identified by the MD simulations also enclose the known positions of crystal water molecules (Figure S3B). Interestingly, we found an extension of this water channel (denoted W_H), which is located between the $4Fe_H$ subsite of the H-cluster and the accessory Fe_S cluster FSA (Figure 1B; Figure S3B). It also connects the Fe_d site with the $4Fe_H$ unit and extends to the protein surface. We hypothesized that O_2 could reach $4Fe_H$ cluster through several channels and finally diffuse through channel W_H to the $2Fe_H$ subsite, where it would initiate the H-cluster degradation process.

Variants G302A, G302S and S357T show WT-like catalytic features

Based on our MD simulation results, we attempted to block W_H between the two H-cluster moieties to prevent the diffusion of O_2 from $4Fe_H$ towards $2Fe_H$. As promising target sites, we identified a glycine residue at position 302 and a serine residue at position 357 about 4 Å away from $4Fe_H$. The G302 carbonyl group forms hydrogen bonds with the backbone amino groups of R305 and Q306. The OH-group of S357 is known to be flexible.^[26] Depending on its orientation, an H-bond is formed with C355. As residues 302 and 357 are located in a potential constriction zone of W_H , we speculated that one could manipulate the diameter of W_H and thus block this short connection pathway between the $4Fe_H$ moiety and the Fe_d subsite. However, the substitutions of uncharged residues in the vicinity of Fe_S clusters for charged ones or vice versa could affect the redox potential and thus influence catalytic performance.^[27] Differences in the catalytic performance have already been identified in a saturation mutagenesis study of S357 of Cpl.^[22] We therefore avoided such exchanges that may have unintended side effects including those that may cause strong steric effects. We instead picked more subtle substituents with slightly larger aliphatic or polar side-chains. The Cpl variants G302S, G302A and S357T were heterologously pro-

duced in *E. coli*. After *in vitro* maturation of the active site,^[28] attenuated total reflectance-fourier transform (ATR-FTIR) spectroscopy revealed close to 100% H-cluster occupancy in all cases (Table S1).

H_2 production activities of the variants provided with sodium dithionite and methyl viologen were comparable to those of the wild type enzyme (G302S: $2841 \pm 347 \mu\text{mol } H_2 \times \text{mg}^{-1} \times \text{min}^{-1}$, G302A: $2355 \pm 213 \mu\text{mol } H_2 \times \text{mg}^{-1} \times \text{min}^{-1}$, S357T: $2543 \pm 315 \mu\text{mol } H_2 \times \text{mg}^{-1} \times \text{min}^{-1}$, WT: $2778 \pm 358 \mu\text{mol } H_2 \times \text{mg}^{-1} \times \text{min}^{-1}$).^[4] Based on Figure S4, no major differences between the variants and the WT can be recognized in the cyclic voltammetry measurements (CV's).

Increased O_2 stability of G302S and S357T

The impact of the described manipulations of W_H on the O_2 sensitivity of the variants was investigated by protein film electrochemistry. Chronoamperometric experiments were employed to record catalytic H_2 oxidation currents before, during and after incubation with O_2 comparable with earlier studies.^[20,29] The catalytic activity of enzymes adsorbed on a PGE (pyrolytic graphite edge) electrode is directly proportional to the measured current.^[30] Differences in current intensity can vary due to different protein coverage of the electrode.^[31]

To enable a comparison between different measurements, each data series was normalized by dividing the recorded current by the calculated synthetic film loss.^[32] Control experiments were performed to determine any dilution effects on the current or the protein film due to the buffer-injection, which were only minor (Figure S5).

Figure 2 shows that the analyzed Cpl enzymes varied notably regarding their sensitivity towards O_2 in a final concentration of 100 μM . While variant G302 A showed similar levels of O_2 tolerance as the WT enzyme, the exchange of G302 to serine and the exchange of S357 to threonine resulted in O_2 -dependent inactivation rates decreased by 20–30% compared to Cpl WT (Figure 2A, Figure S6). Remarkably, 5 min after the injection of O_2 the residual activities of G302S and S357T were still above 50%, demonstrating the significant O_2 tolerance of both variants. However, the Cpl S357T variant identified in the mentioned screening study showed $\approx 210\%$ of the Cpl wild type performance in the *in vitro* H_2 -production activity assays in presence of O_2 .^[23]

These and our results, obtained by different methodical approaches, thus support each other well and verify that S357 plays an important role for O_2 tolerance in Cpl. Here, to eliminate the factor of competition between H_2 - (substrate) and O_2 - (inhibitor) diffusion under H_2 oxidation conditions^[29] and to confirm a higher resistance against O_2 of variants G302S and S357T, we also incubated the protein films for 30 s, 1 min or 2 min in O_2 -saturated buffer in the absence of any applied potential. In line with the preceding results the residual activities of G302S and S357T in reference to their activities prior to O_2 exposure were 10–15% higher than those of Cpl WT (Figure 2B, Figures S7–9). Calculated half-life values of the enzymes under these specific conditions are for WT: 18.6 ± 1.1 s,

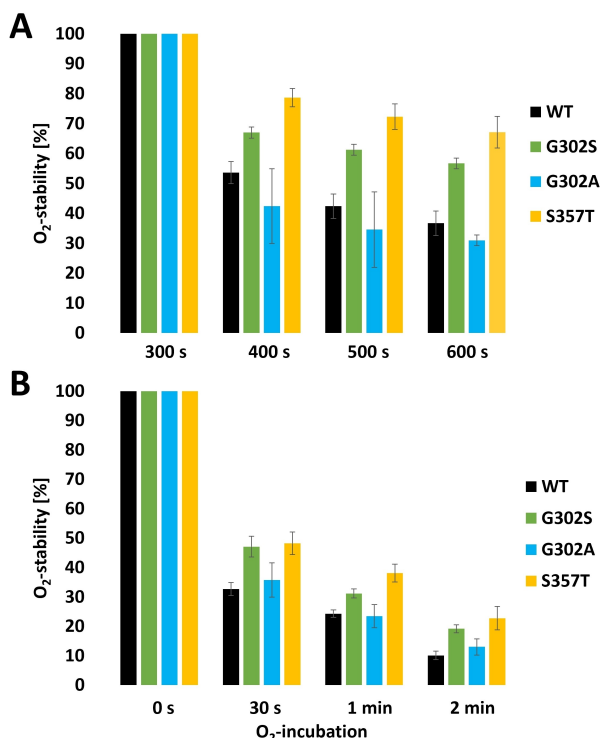


Figure 2. Chronoamperometry measurements to verify the O₂ tolerance (A) and O₂ resistance (B) of Cpl WT protein (black) compared to the variants G302S (green), G302A (blue) and S357T (yellow): A. Percentage of H₂ oxidation activity of all proteins before (time point: 300 s) and after (time points: 400 s; 500 s; 600 s) an injection of O₂-saturated buffer into the cell, resulting in a final concentration of O₂ of 100 μM. Data for each time point were extracted from continuous measurements shown in Figure S6. B. The effect of O₂ on the H₂ oxidation current of all proteins before (0 s) and after incubation in O₂-saturated buffer for the indicated time periods. The protein film on the graphite electrode was slowly dipped into O₂-saturated buffer and incubated for 30 s, 1 min or 2 min. Afterwards, the electrode was reconnected to the rotator and residual H₂ oxidation current in anoxic buffer was measured followed by a normalization of the data (Figure S9). Experimental conditions were as follows: All proteins were adsorbed onto a graphite electrode rotating at 3000 rpm; potential (E) = −44 mV vs SHE, buffer at pH 7, temperature = 10 °C, constant stream of 30 L·min^{−1} of 100% H₂. Columns represent mean values of two biological and three technical replicates, error bars indicate the standard deviation.

for G302A 20.4 ± 3.0 s, for G302S: 27.8 ± 2.8 s and for S357T: 28.7 ± 2.9 s. Here, we also combined both exchanges in a single Cpl variant (G302S-S357T), but we could not detect a synergistic effect after incubating the adsorbed protein in O₂-saturated buffer (Figure S10A). In addition, we also investigated the O₂-stability of S357T and G302S in H₂-production direction and confirmed the 10–15% O₂-stability of the H₂-oxidation direction (Figure S10B, C).

Structural elucidation confirms changes in the side-chain architecture of variants G302S and S357T

To decipher the molecular basis of the observed differences in O₂ stability, we determined the crystal structure of G302S at 1.63 Å resolution and of S357T at 1.60 Å resolution (Table S2). The structures of the protein variants were compared to the

structure of WT-Cpl. The overall structures of G302S and S357T are very similar to the structure of the WT enzyme (Figure S11A). The root-mean-square deviations of Cα-atoms relative to WT-Cpl (4XDC^[12]) are 0.703 Å and 0.696 Å for G302S and S357T, respectively. Any notable differences in side-chain orientations of the variants were limited to surface exposed residues and side-chain S357 (Figure S11). Notably, the exchange of G302 by serine allowed the formation of two additional H-bonds, formed by the side-chain hydroxyl group of the new S302 residue. One H-bond is formed with the backbone carbonyl of L191 and one with the hydroxyl group of S357. Since the WT enzyme is more sensitive to O₂, it is tempting to speculate that these additional H-bonds in variant G302S might influence the flexibility of the protein region and thus alter the diffusion of molecules, including O₂, along the W_H pathway.

The exchange of serine 357 to the bulkier threonine likely results in a restricted side-chain flexibility. Interestingly the exchange of glycine 302 to the bulkier serine affects the side-chain conformation of S357 in both chains A and B of the crystal structure. The newly introduced possibility to establish an H-bond contact between both hydroxy groups appears to lock the side-chain of S357 in the conformation most suitable for a stable H-bond contact (Figure S11B).

MD simulations show blockage of W_H in variants G302S and S357T

To investigate the influence of the amino acid exchanges in variants G302S and S357T on the water channel network surrounding the H-cluster and to analyze a possible blockage of W_H, MD simulations were performed as described above for wild type Cpl. Figure 3 shows that in the variant G302S, the W_H channel is interrupted in direct vicinity to the 4Fe_H subsite of the H-cluster close to the exchanged amino acid residue (compare Figure 3A and Figure 3B). This interruption of the channel is due to the formation of a tight H-bond network formed by the side-chain of S302, the peptide backbone of L191 and one side-chain conformation of S357 (Figure 3E). A similar constriction of the channel is found in the S357T variant (Figure 3C), in which the local network rearranges such that an H-bond is formed between the

hydroxyl group of T357 and the backbone carbonyl group of L192 (Figure 3F). These changes also lead to the formation of a 'hydrophobic cluster' comprised of the side-chain of L192 and the methyl group of T357, which interrupts W_H at that local region (Figure 3C). Combined with the experimental results described above, the MD simulations show that both exchanges, G302S and S357T, effectively block the (same) hydrophilic channel connecting 2Fe_H and 4Fe_H due to the introduction of channel-constricting H-bond networks. These structural rearrangements reduce the diameter of the putative diffusion channel and thus lead to an enhanced molecular sieving effect that shields (or protects) the H-cluster against O₂ to a certain extent. This study shows for the first time the influence of the specific hydrophilic channel-region on the O₂ stability, which explains why Koo and coworker's study assumed a new O₂

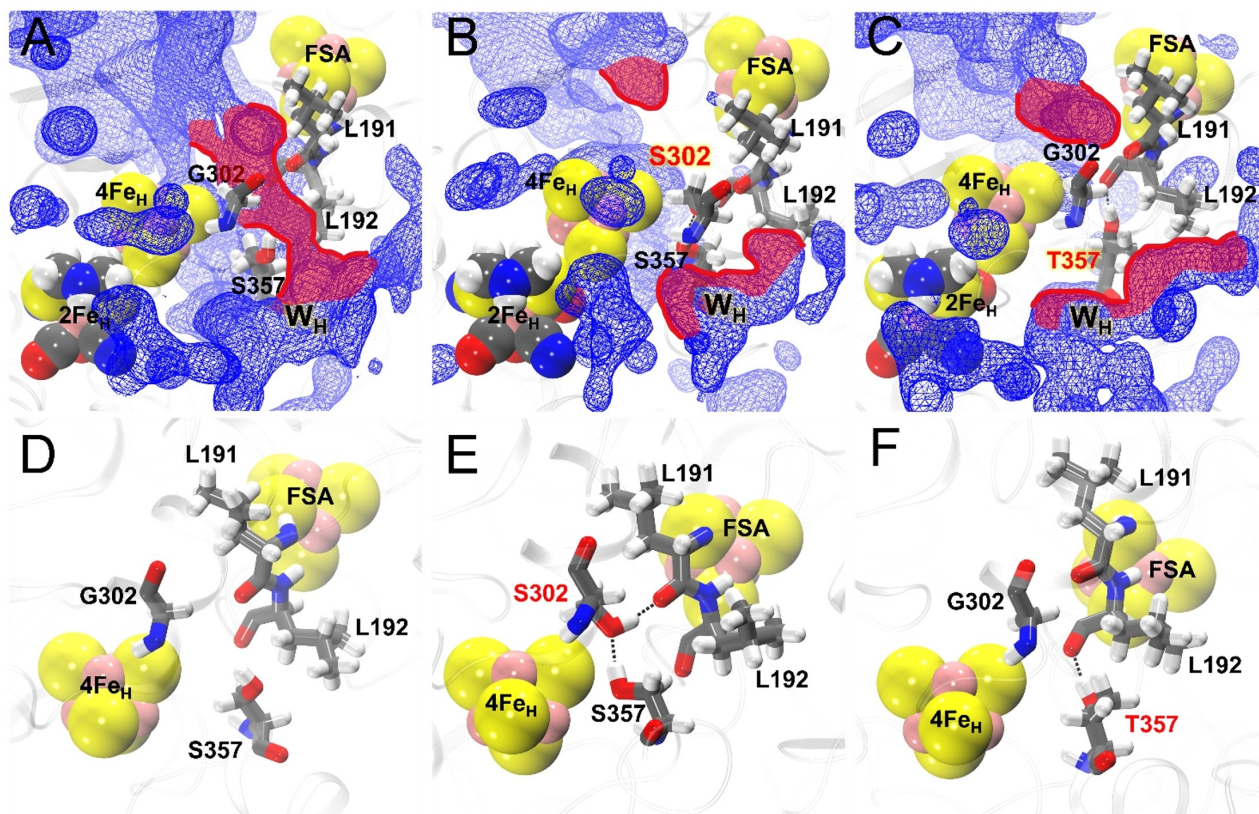


Figure 3. Volumetric maps showing the three-dimensional water occupancy based on MD simulations of Cpl WT (A), variant G302S (B), and variant S357T (C). The described region of W_H is highlighted in red for all three proteins. A local interruption of the water density in W_H can be seen close to positions S302 (B) and T357 (C). Compared to the structure of the wild type enzyme (D) S302 forms H-bonds with the backbone carbonyl of L191 and the hydroxyl group of S357 in case of the G302S variant (E), whereas the hydroxyl group of T357 forms an H-bond with the backbone of L192 in the S357T variant (F). In both cases, this leads to blockage of the W_H channel. Other open tunnel cavities are not affected by the local rearrangement of H-bond networks in the two analyzed Cpl variants.

stability mechanism for the more O_2 -stable variants S357T and at the same time did not consider nearby affected hydrophilic diffusion channels.^[23] At this point we are unable to differentiate whether the changes of Cpl block the diffusion of O_2 from the surface via the $4Fe_H$ cluster to the $2Fe_H$ site, or whether they also hinder the diffusion of ROS from the site of O_2 activation at the $2Fe_H$ substrate binding site to the $4Fe_H$ subcluster. Both could explain the observed impact on the O_2 resistance of the two enzyme variants. In any case the H-cluster is only partially protected, probably because i) the destruction of the $2Fe_H$ subcluster cannot be prevented by only manipulating the W_H , and ii) $4Fe_H$ is still connected to the bulk solvent through additional channels and is thus still susceptible to destruction through these additional routes.

Conclusions

MD simulations based on high-resolution crystal structures were used to study dynamic exchanges of water molecules in [FeFe]-hydrogenases and allowed us to identify a new water channel, W_H , around the H-cluster. The simulations also confirmed that local blockages of W_H increase the O_2 stability of Cpl. This was achieved by amino acid exchanges, G302S and

S357T, which both individually decreased protein flexibility close to residue 357 in the vicinity of $4Fe_H$ by redesigning the local H-bond network. While O_2 diffusion from the surface to $2Fe_H$ via gas channel A or B and subsequent binding to Fe_d have already been shown to be difficult to prevent,^[13,17,33] we partially blocked the diffusion of O_2 from $4Fe_H$ to the $2Fe_H$ subcluster and identified this influential hydrophilic region. Significant improvements of O_2 stability could be reached by single amino acid exchanges based on electrochemical measurements. Enhancing the molecular sieve effect in the immediate protein environment of the H-cluster may be more effective than trying to constrict individual gas channel branches in the outer protein shell.

Experimental Section

Site-directed mutagenesis. To generate hydrogenase-encoding sequences with modified codons, the Quik Change method was employed.^[34] Mismatch primer pairs (ordered at Sigma-Aldrich) were used to amplify the expression plasmid pET21b-Cpl (Table S3). The parental DNA template was digested (*DpnI*; Thermo Fisher Scientific) and the PCR product was introduced into *Escherichia coli* DH5 α using the heat-shock method.

Expression and purification. For the expression of Cpl apo-hydrogenases sequences, the expression plasmids with the respective hydrogenase sequences were introduced into *E. coli* strain BL21 (DE3) Δ iscR.^[35] Expression and subsequent protein purification was done as already reported.^[36] Briefly, all proteins (equipped with a C-terminal Strep-tagII) were purified by affinity chromatography using Strep-Tactin® Superflow® columns (IBA GmbH). Proteins were eluted in 0.1 M Tris-HCl pH 8, supplemented with 2.5 mM desthiobiotin and 2 mM sodium dithionite (NaDT). Protein quantity and quality were analyzed employing the Bradford assay^[37] and by standard SDS-PAGE (sodium dodecylsulfate-polyacrylamide gel electrophoresis) (Bio-Rad)^[38]. The isolated proteins were stored in air-tight glass vessels at -80°C until further use. To avoid O_2 contamination during experiments, Coy Laboratory Anaerobic vinyl tents with an atmosphere of 98.5% N_2 and 1.5% H_2 were used.

In vitro maturation of [FeFe]-hydrogenases. Purified apo-Cpl proteins, lacking the 2Fe_H -subcluster, were matured *in vitro* with the synthetic mimic of the native 2Fe_H -complex ($\text{Fe}_2[\mu\text{-(SCH}_2)_2\text{NH}](\text{CN})_2(\text{CO})_4[\text{Et}_4\text{N}]_2$) ($[\text{2FeH}]^{\text{MIM}}$) as reported before^[28,39]. Briefly, the proteins were incubated with a 10-fold molar excess of 2FeH^{MIM} for 1 h on ice in 0.1 M potassium phosphate buffer (KPI) pH 6.8. Excess $2\text{Fe}_\text{H}^{\text{MIM}}$ was removed by size exclusion chromatography employing NAP 5 columns (GE healthcare).

In vitro H_2 production assay. To determine the specific H_2 production activities of wild type Cpl and variants, 400 ng of holo proteins in 0.1 M KPI pH 6.8 were mixed with methyl viologen (MV) as an electron mediator (10 mM) and NaDT as sacrificial electron donor (100 mM) in 8-ml headspace vials. The vials were sealed airtight with red Suba-Seal septa and the headspace of each vial was purged with 100% argon for 5 min. After incubating the reaction mixtures in a shaking water bath (100 rpm) at 37°C for 20 minutes, H_2 was quantified in 400 μl of the headspace of each sample by gas chromatography (GC-2010, Shimadzu).

Crystallization and structural analysis. The hanging drop vapour diffusion technique was used to crystallize Cpl proteins ($15\text{ mg} \times \text{ml}^{-1}$) in an anoxic atmosphere at 4°C . The procedure was carried out as previously described.^[4,14] After 10–14 days of growth, the crystals were mounted and flash frozen in liquid N_2 . Diffraction data were collected on beamlines ESRF ID30B or ESRF ID30 A (Grenoble, France) at 100 K. The processing of the data was done with XDS.^[40] Molecular replacement and refinement for site-directed mutagenesis variants were done with Phenix^[41] and Coot.^[42] The statistics of crystallographic data are summarized in Table S2. The coordinates and structure factors were deposited in PDB (protein data bank) as entries 7QHF (G302S) and 8CJY (S357T).

Infrared spectroscopy. Attenuated total reflectance-fourier transform spectroscopy (ATR-FTIR-spectroscopy) was recorded anoxically for wild type (WT) Cpl and its variants by using a Tensor II spectrometer (Bruker Optik, Germany), with a BioATR cell II (Harrick) which consists of a double reflecting ZnSE/Si crystal. The spectra were recorded after a semi-drying process of the protein film. A N_2 gas stream passed through a buffer compartment containing 0.1 M Tris-HCl, pH 8, was applied to re-humidify the protein film on the crystal. The measurement was recorded from 4000–1000 cm^{-1} with 2 cm^{-1} resolution at room temperature. The program OPUS (Bruker GmbH) was used for baseline correction and OriginPro (Origin Lab) for plotting the spectra. Morra and coworker have recently shown state specific signals for Cpl, which were used for orientation.^[43] The calculation of the cluster occupancy was done as described in Lampret et al (2019).^[44]

Protein-film-electrochemical experiments (PFE). PFE were performed with an electrochemical cell employing three electrodes as reported previously^[20] in an anoxic atmosphere in a vinyl tent as

described above. All electrochemical experiments were conducted with an electrode rotation speed of 3000 rpm, a 30 $\text{L} \times \text{min}^{-1}$ H_2 gas stream, a temperature of 10°C and at pH 7. Cyclic voltammetry scans were recorded at a scan rate of 5 mV/s. For the two used chronoamperometric measurements (O_2 -tolerance test; O_2 -resistance test) a normalization was done for each data series in OriginPro regarding the difference in protein film loss over time. For this, the exponential decay function ExpDec 1 was used. This normalization procedure is orientated on the work of Fourmond et al. 2009.^[32] For the O_2 -tolerance test O_2 saturated buffer was injected into the cell after 300 s leading to a final concentration of 100 μM of O_2 . In case of the O_2 -resistance test the electrode with adsorbed protein was incubated into O_2 -saturated buffer for a specific time frame (30 s–2 min). For more information see Supporting information section 1.

Molecular dynamics. All molecular dynamics (MD) simulations were carried out with the GROMACS program package, version 2019.2.^[45] The starting structures of the G302S and S357T Cpl [FeFe]-hydrogenase variants were taken from the X-ray crystal structures reported in this work (7QHF and 8CJY, respectively); for wild-type Cpl the previously published X-ray structure (4XDC)^[12] was used.

The CHARMM36 protein force field was used together with the CHARMM-specific TIP3P water model.^[46] The H_{ox} state of Cpl was simulated in the present work. The force field parameters for the H-cluster and the accessory FeS clusters, including the ligating Cys and His residues, were taken from the work of Chang et al.^[47] with the additional modifications suggested by McCullagh and Voth.^[48] Each protein was fully solvated with 27388 water molecules; all crystal water molecules were kept in the simulation setup. The MD simulations were conducted with periodic boundary conditions using dodecahedron-shaped simulation boxes that comprised a total of 91231 atoms for WT, 91235 atoms for G302S, and 91234 atoms for S357T Cpl (including protein, FeS clusters, water molecules, and Na^+ ions to neutralize the systems).

Prior to the production of MD simulations, the systems were energy-minimized (1000 steepest descent steps) followed by step-wise equilibration for 2.7 ns, during which harmonic position restraining potentials were applied to different sets of atoms. During the initial NVT equilibration phase (0.2 ns), position restraints with force constants of 1000 kJ/mol/nm² were applied to all non-hydrogen atoms of the protein and the FeS clusters. Second, the equilibration was continued for another 2.5 ns in the NpT ensemble. During the first 0.5 ns of this second equilibration phase, the position restraints were still applied to all non-hydrogen atoms of the protein and the FeS clusters. Then, during the final 2.0 ns, the position restraints were only applied to all non-hydrogen atoms of the protein backbone. The temperature was kept constant at 300 K during the MD simulations by coupling to the velocity rescaling thermostat of Bussi and coworkers^[49] with a coupling time constant of 0.1 ps. Constant 1 bar pressure was maintained in the NpT simulations by using a weak coupling barostat^[50] with a coupling time constant of 2 ps and a compressibility of $4.5 \times 10^{-5} \text{ bar}^{-1}$. The short-range Coulomb and Lennard-Jones 6,12 interactions were described with a buffered Verlet pair list^[51] with potentials smoothly shifted to zero at a 1.2 nm cutoff, with the forces smoothly switched to zero between 1.0 and 1.2 nm. The long-range electrostatic interactions were treated with the particle mesh Ewald (PME) method with 0.12 nm grid spacing.^[52] The LINCS^[53] and SETTLE^[54] constraint algorithms were employed to constrain all protein bonds involving H-atoms and all internal degrees of freedom of water molecules, respectively, allowing to integrate the equations of motion with 2 fs time steps. Finally, using the equilibrated simulation systems as starting conditions, three 1000 ns production simulations were carried out within the NpT ensemble at 300 K, for each of the three proteins simulated

(WT, G302S and S357T). Different random seeds were used to generate the initial atomic velocities from a Maxwell-Boltzmann distribution.

Acknowledgements

This project received funding from the Research Training Group GRK 2341 "Microbial Substrate Conversion (MiCon)". The authors are grateful for the technical support during X-ray data collection in ESRF and DESY. JD acknowledges the financial support from DFG (project number 461338801). This project received funding from the European Union's Horizon2020 research and innovation programme under the Marie Skłodowska-Curie grant agreement No 801459 – FP-RESOMUS and from the Deutsche Forschungsgemeinschaft (DFG) under Germany's Excellence Strategy – EXC 2033 – 390677874 – RESOLV. T.H. thanks Volkswagen Stiftung (Az 98621) and the DFG for funding (HA 2555/10-1). Open Access funding enabled and organized by Projekt DEAL.

Conflict of Interests

The authors declare no conflict of interest.

Data Availability Statement

The data that support the findings of this study are available from the corresponding author upon reasonable request.

Keywords: hydrogenase · gas channels · molecular dynamics · oxygen · hydrogen bonds

- [1] F. A. Armstrong, J. Hirst, *Proc. Natl. Acad. Sci. USA* **2011**, *108*, 14049–14054.
- [2] G. Caserta, et al., *J. Am. Chem. Soc.* **2018**, *140*, 5516–5526.
- [3] J. W. Peters, G. J. Schut, E. S. Boyd, D. W. Mulder, E. M. Shepard, J. B. Broderick, P. W. King, M. W. W. Adams, *Biochim. Biophys. Acta.* **2015**, *1853*, 1350–1369.
- [4] J. Duan, M. Senger, J. Esselborn, V. Engelbrecht, F. Wittkamp, U.-P. Apfel, E. Hofmann, S. T. Stripp, T. Happe, M. Winkler, *Nat. Commun.* **2018**, *9*, 4726.
- [5] H. Long, P. W. King, C. H. Chang, *J. Phys. Chem. B* **2014**, *118*, 890–900.
- [6] G. Hong, A. J. Cornish, E. L. Hegg, R. Pachter, *Biochim. Biophys. Acta.* **2011**, *1807*, 510–517.
- [7] J. Cohen, K. Kim, P. King, M. Seibert, K. Schulten, *Structure* **2005**, *13*, 1321–1329.
- [8] A. R. Finkelmann, M. T. Stiebritz, M. Reiher, *Inorg. Chem.* **2014**, *53*, 11890–11902.
- [9] A. Kubas, et al., *Nat. Chem.* **2017**, *9*, 88–95.
- [10] S. Mebs, et al., *Biochim. Biophys. Acta Bioenerg.* **2018**, *1859*, 28–41.
- [11] J. Noth, R. Kositzki, K. Klein, M. Winkler, M. Haumann, T. Happe, *Sci. Rep.* **2015**, *5*, 13978.
- [12] J. Esselborn, N. Muraki, K. Klein, V. Engelbrecht, N. Metzler-Nolte, U.-P. Apfel, E. Hofmann, G. Kurisu, T. Happe, *Chem. Sci.* **2016**, *7*, 959–968.
- [13] T. Lautier, P. Ezanno, C. Baffert, V. Fourmond, L. Cournac, J. C. Fontecilla-Camps, P. Soucaille, P. Bertrand, I. Meynial-Salles, C. Léger, *Faraday Discuss.* **2011**, *148*, 385–407; discussion 421–41.
- [14] J. Esselborn, L. Kertess, U.-P. Apfel, E. Hofmann, T. Happe, *J. Am. Chem. Soc.* **2019**, *141*, 17721–17728.
- [15] a) M. T. Stiebritz, M. Reiher, *Inorg. Chem.* **2009**, *48*, 7127–7140; b) K. D. Swanson, et al., *J. Am. Chem. Soc.* **2015**, *137*, 1809–1816.
- [16] M. K. Bruska, M. T. Stiebritz, M. Reiher, *J. Am. Chem. Soc.* **2011**, *133*, 20588–20603.
- [17] P.-P. Liebgott et al., *Nat. Chem. Biol.* **2010**, *6*, 63–70.
- [18] S. T. Stripp, G. Goldet, C. Brandmayr, O. Sanganas, K. A. Vincent, M. Haumann, F. A. Armstrong, T. Happe, *Proc. Natl. Acad. Sci. USA* **2009**, *106*, 17331–17336.
- [19] J. Cohen, K. Kim, M. Posewitz, M. L. Ghirardi, K. Schulten, M. Seibert, P. King, *Biochem. Soc. Trans.* **2005**, *33*, 80–82.
- [20] M. Winkler, et al., *Nat. Commun.* **2021**, *12*, 756.
- [21] S. Zacarias, A. Temporão, M. Del Barrio, V. Fourmond, C. Léger, P. M. Matias, I. A. C. Pereira, *ACS Catal.* **2019**, *9*, 8509–8519.
- [22] a) T. Goris, et al., *Nat. Chem. Biol.* **2011**, *7*, 310–318; b) C. Orain, L. Saujet, C. Gauquelin, P. Soucaille, I. Meynial-Salles, C. Baffert, V. Fourmond, H. Bottin, C. Léger, *J. Am. Chem. Soc.* **2015**, *137*, 12580–12587.
- [23] J. Koo, J. R. Swartz, *Metab. Eng.* **2018**, *49*, 21–27.
- [24] a) P. Wang, R. B. Best, J. Blumberger, *Phys. Chem. Chem. Phys.* **2011**, *13*, 7708–7719; b) A. S. Bingham, P. R. Smith, J. R. Swartz, *Int. J. Hydrogen Energy* **2012**, *37*, 2965–2976.
- [25] M. Mohammadi, H. Vashisth, *J. Phys. Chem. B* **2017**, *121*, 10007–10017.
- [26] J. H. Artz, et al., *J. Am. Chem. Soc.* **2020**, *142*, 1227–1235.
- [27] a) M. Heghmanns, A. Günzel, D. Brandis, Y. Kutin, V. Engelbrecht, M. Winkler, T. Happe, M. Kasanmascheff, *Biophys. Rep.* **2021**, *1*, 100016; b) A. Kubas, D. De Sancho, R. B. Best, J. Blumberger, *Angew. Chem.* **2014**, *126*, 4165–4168; c) E. J. Brooke, R. M. Evans, S. T. A. Islam, G. M. Roberts, S. A. M. Wehlin, S. B. Carr, S. E. V. Phillips, F. A. Armstrong, *Biochemistry* **2017**, *56*, 132–142.
- [28] J. Esselborn, et al., *Nat. Chem. Biol.* **2013**, *9*, 607–609.
- [29] G. Goldet, C. Brandmayr, S. T. Stripp, T. Happe, C. Cavazza, J. C. Fontecilla-Camps, F. A. Armstrong, *J. Am. Chem. Soc.* **2009**, *131*, 14979–14989.
- [30] M. Del Barrio, M. Sensi, C. Orain, C. Baffert, S. Dementin, V. Fourmond, C. Léger, *Acc. Chem. Res.* **2018**, *51*, 769–777.
- [31] N. Kornienko, K. H. Ly, W. E. Robinson, N. Heidary, J. Z. Zhang, E. Reisner, *Acc. Chem. Res.* **2019**, *52*, 1439–1448.
- [32] V. Fourmond, et al., *Anal. Chem.* **2009**, *81*, 2962–2968.
- [33] F. Leroux, et al., *Proc. Natl. Acad. Sci. USA* **2008**, *105*, 11188–11193.
- [34] L. Zheng, U. Baumann, J.-L. Reymond, *Nucleic Acids Res.* **2004**, *32*, e115.
- [35] M. K. Akhtar, P. R. Jones, *Appl. Microbiol. Biotechnol.* **2008**, *78*, 853–862.
- [36] J. M. Kuchenreuther, C. S. Grady-Smith, A. S. Bingham, S. J. George, S. P. Cramer, J. R. Swartz, *PLoS One* **2010**, *5*, e15491.
- [37] M. M. Bradford, *Anal. Biochem.* **1976**, *72*, 248–254.
- [38] U. K. Laemmli, *Nature* **1970**, *227*, 680–685.
- [39] H. Li, T. B. Rauchfuss, *J. Am. Chem. Soc.* **2002**, *124*, 726–727.
- [40] W. Kabsch, *Acta Crystallogr. Sect. D* **2010**, *66*, 125–132.
- [41] P. D. Adams, et al., *Acta Crystallogr. Sect. D* **2010**, *66*, 213–221.
- [42] P. Emsley, K. Cowtan, *Acta Crystallogr. Sect. D* **2004**, *60*, 2126–2132.
- [43] S. Morra, J. Duan, M. Winkler, P. A. Ash, T. Happe, K. A. Vincent, *Dalton Trans.* **2021**, *50*, 12655–12663.
- [44] O. Lampret, et al., *Proc. Natl. Acad. Sci. USA* **2019**, *116*, 15802–15810.
- [45] M. J. Abraham, T. Murtola, R. Schulz, S. Páll, J. C. Smith, B. Hess, E. Lindahl, *SoftwareX* **2015**, *1–2*, 19–25.
- [46] R. B. Best, X. Zhu, J. Shim, P. E. M. Lopes, J. Mittal, M. Feig, A. D. Mackerell, *J. Chem. Theory Comput.* **2012**, *8*, 3257–3273.
- [47] C. H. Chang, K. Kim, *J. Chem. Theory Comput.* **2009**, *5*, 1137–1145.
- [48] M. McCullagh, G. A. Voth, *J. Phys. Chem. B* **2013**, *117*, 4062–4071.
- [49] G. Bussi, D. Donadio, M. Parrinello, *J. Chem. Phys.* **2007**, *126*, 14101.
- [50] H. J. C. Berendsen, J. P. M. Postma, W. F. Van Gunsteren, A. DiNola, J. R. Haak, *J. Chem. Phys.* **1984**, *81*, 3684–3690.
- [51] S. Páll, B. Hess, *Comput. Phys. Commun.* **2013**, *184*, 2641–2650.
- [52] U. Essmann, L. Perera, M. L. Berkowitz, T. Darden, H. Lee, L. G. Pedersen, *J. Chem. Phys.* **1995**, *103*, 8577–8593.
- [53] B. Hess, *J. Chem. Theory Comput.* **2008**, *4*, 116–122.
- [54] S. Miyamoto, P. A. Kollman, *J. Comput. Chem.* **1992**, *13*, 952–962.

Manuscript received: September 19, 2023

Revised manuscript received: October 5, 2023

Accepted manuscript online: October 13, 2023

Version of record online: November 17, 2023